# Finite-Difference Implementation of Inviscid Separated Flows with Infinitely-Long Cusp-Ended Stagnation Zone around Circular Cylinder

# M. D. Todorov

Dept. of Differential Equations, Institute of Mathematics and Informatics, Technical University of Sofia, Sofia 1756, Bulgaria e-mail: mtod@vmei.acad.bg

#### Abstract

The classical Helmholtz problem is applied for modelling and numerical investigation of inviscid cusp-ended separated flow around circular cylinder. Two coordinate systems are used: polar for initial calculations and parabolic as topologically most suited for infinite stagnation zone. Scaling by the shape of the unknown free line renders the problem to computational domain with fixed boundaries. Difference schemes and algorithm for Laplace equation and for Bernoulli integral are devised. A separated flow with drag coefficient  $C_x = 0$  like the so called "critical" flow is obtained. The pressure distribution on the surface of cylinder and the detachment point compares quantitatively very well with the predictions of the hodograph method.

# 1. Introduction

In 1868 Helmholtz [11] introduces the notion of a flow consisting of a potential and stagnant zones matching at priori unknown free boundaries which are tangential discontinuities and where the balance of normal stresses (the pressure) holds. Kirchhoff [13] came up with the first solution for the ideal flow around flat plate when the detachment points were known in advance. Later on in the turning of our century, Levi-Civita [14], Villat [19] etc. developed further the hodograph method and demonstrated its application to flows around curved bodies. Satisfying an additional condition for smooth separation (called now Brillouin-Villat condition [1, 19, 20]) Brodetsky [2] obtained by the hodograph method approximate solution for the circular cylinder with a parabolic expanding at infinity shape of the stagnation zone.

In the years 40 of the present century with the computer advent it was already possible to calculate such class of flows direct at the physical plane. The first calculations [12, 17] gave interesting results. Along with the Brodetsky flow a radically different Helmholtz flow takes place with decreasing stagnation zone which forms at infinity cusp [3]. Because of the limitation of computers the shape of the zone was not conclusive. It appears that the method of hodograph can also be applied to obtain such a flow (see, e.g., [10]) but

only for the case of circular cylinder. We also found such cusp-ended stagnation zones [5, 6, 7] by means of difference scheme and confirmed by integral-method calculations [18]. A new interesting solution for the shape of the wake behind the circular cylinder was obtained after further modifying of the difference scheme. Preliminary results of this study are represented in [8]. The features of the algorithm and our further investigation will be discussed here.

# 2. Posing the Problem

Consider the steady inviscid flow past a circle – the cross section of an infinitely long circular cylinder. The direction of the flow coincides with the line  $\theta = 0, \pi$  of the polar coordinates and the leading stagnation point of the flow is situated in the point  $\theta = \pi$ . Taking into account the symmetry with respect to the line  $\theta = 0, \pi$  we consider the flow only in upper half plane.

#### 2.1. Coordinate Systems

The gist of our approach is to make use of two different coordinate systems: the polar one (turning out to be ineffective for the case of infinite stagnation zones extending far away from the rear end of body) and the parabolic one the latter being topologically more suited for solving Laplace equation outside infinitely long stagnation zones. We initiate the calculations in polar coordinates switching to parabolic coordinates after the stagnation zone has fairly well developed and has become long enough.

In terms of the two coordinate systems (cylindrical and parabolic) Laplace equation for the stream function  $\psi$  reads:

$$\frac{1}{r}(r\psi_r)_r + \frac{1}{r^2}\psi_{\theta\theta} = 0$$
, or  $\frac{1}{\sigma^2 + \tau^2}(\psi_{\sigma\sigma} + \psi_{\tau\tau}) = 0$ . (2.1)

The undisturbed uniform flow at infinity is given by

$$|\psi|_{r\to\infty} \approx rU_{\infty} \sin \theta$$
, or  $|\psi|_{\sigma\to\infty,\,\tau\to\infty} \approx \sigma\tau U_{\infty}$ . (2.2)

On the combined surface "body+stagnation zone" hold two conditions. The first condition secures that the said boundary is a stream line (say of number "zero")

$$\psi(R(\theta), \theta) = 0, \ \theta \in [0, \pi] \quad \text{or} \quad \psi(S(\tau), \tau) = 0, \ \tau \in (0, \infty),$$
 (2.3)

where  $R(\theta)$ ,  $S(\tau)$  are the shape functions of the total boundary in polar or parabolic coordinates, respectively. Here and henceforth we use the notation  $\Gamma_1$  for the portion of boundary representing the cylinder and  $\Gamma_2$  – for the free streamline (Fig.1).

Let  $\theta^*$  and  $\tau^*$  be the magnitudes of the independent coordinates for which the detachment of flow occurs. As far as we consider only the case when the stagnation zone is situated behind the body then the portion of  $\Gamma_2$  which describes the free line of the flow is defined as  $0 \le \theta \le \theta^*$  or  $\tau \ge \tau^*$ , respectively. On  $\Gamma_2$  the shape function  $R(\theta)$  is unknown and it is to be implicitly identified from Bernoulli integral with the pressure equal to a constant (say,  $p_c$ ) which is the second condition holding on the free boundary.

For the two coordinate systems one gets the following equations for shape functions  $R(\theta)$  or  $S(\tau)$ :

$$\left[q + \frac{\psi_{\theta}^{2}}{r^{2}} + \psi_{r}^{2}\right]_{r=R(\theta)} = 1, \quad \text{or} \quad \left[q + \frac{\psi_{\sigma}^{2} + \psi_{\tau}^{2}}{\sigma^{2} + \tau^{2}}\right]_{\sigma=S(\tau)} = 1. \quad (2.4)$$

$$0 \le \theta \le \theta^{*}, \quad \tau^{*} < \tau < \infty,$$

where q is a dimensionless pressure.

At the symmetry line  $\theta = 0, \pi$  additional conditions are added

$$\frac{\partial \psi}{\partial \theta} = 0 , \ \theta = 0, \pi \quad \text{or} \quad \frac{\partial \psi}{\partial \tau} = 0 , \ \tau = 0 .$$
 (2.5)

and thus (2.1), (2.2), (2.3), (2.4) and (2.5) complete b.v.p. for stream-function  $\psi$ .

#### 2.2. Scaled Variables

The above stated boundary value problem is very inconvenient for numerical treatment mainly because of two reasons. The first is that the boundary lines are not coordinate lines. The second is that the shape function of the stagnation zone must be implicitly identified from the additional boundary condition (2.4). Following [9] we scale the independent variable ( $\theta$  or  $\tau$ ) by the shape function  $R(\theta)$  or  $S(\tau)$ :

$$\eta = rR^{-1}(\theta), \qquad \eta = \sigma - S(\tau).$$

Such a manipulation renders the original physical domain under consideration into a region with fixed boundaries, the latter being coordinate lines. In addition the Bernoulli integral becomes an explicit equation for the shape function of the free boundary. Scaling the independent variable proved very efficient in numerical treatment of inviscid or viscous flows with free boundaries (for details see, e.g., [6]).

We treat the two coordinate systems in an uniform way denoting  $\xi \equiv \theta$  or  $\xi \equiv \tau$  depending on the particular case under consideration. In terms of the new coordinates  $(\eta, \xi)$ , the stream function is a compound function  $\tilde{\psi}(\eta, \theta) \equiv \psi(r(\eta, \xi), \xi)$  or  $\tilde{\psi}(\eta, \tau) \equiv \psi(\sigma(\eta, \xi), \xi)$  but in what follows we drop the "tilde" without fear of confusion. The Laplace equation takes then the form

where

$$(a\psi_{\eta})_{\eta} + (b\psi_{\xi})_{\xi} - (c\psi_{\xi})_{\eta} - (c\psi_{\eta})_{\xi} = 0$$

$$a \equiv \eta \left[ 1 + \left( \frac{R'}{R} \right)^{2} \right], \quad b \equiv \frac{1}{\eta}, \quad c \equiv \frac{R'}{R};$$
or
$$a \equiv 1 + S'^{2}, \quad b \equiv 1, \quad c \equiv S'.$$

with respective boundary conditions (see [8]).

Thus we define a well posed boundary value problem for  $\psi$  provided that functions  $R(\theta)$  and  $S(\tau)$  are known. On the other hand in the portion  $\Gamma_2$  of the boundary (where these functions are unknown) they can be evaluated from the Bernoulli integral (2.4) which now becomes an explicit equation for the shape function

$$\frac{R^2 + R'^2}{R^4} \left[ \frac{\partial \bar{\psi}}{\partial \eta} \Big|_{\eta=1} + R(\theta) \sin \theta \right]^2 = 1, \quad \text{or} \quad \frac{1 + S'^2}{S^2 + \tau^2} \left[ \frac{\partial \bar{\psi}}{\partial \eta} \Big|_{\eta=0} + \tau \right]^2 = 1, \quad (2.7)$$

$$0 \le \theta \le \theta^*, \qquad \tau^* \le \tau < \infty.$$

### 3. Forces Exerted on the Body

The presence of a stagnation zone breaks the symmetry of the integral for the normal stresses and hence D'Alembert paradox ceases to exist, i.e. the force exerted from the flow upon the body is no more equal to zero. Denote by n the outward normal vector to the contour  $\Gamma$ . Then the force acting upon the contour is given by

$$\mathbf{R} = -\oint_{\Gamma} p\mathbf{n}ds = -\oint_{\Gamma} (q + p_c)\mathbf{n}ds \stackrel{\text{def}}{=} \rho a U_{\infty}^2 \left[ C_x \mathbf{i} + C_y \mathbf{j} \right] , \qquad (3.1)$$

where  $C_x$  and  $C_y$  are the dimensionless drag coefficient and the lifting force.

After obvious manipulations we obtain for the drag and lifting-force coefficients the following expression (see [8])

$$C_{x} = -2 \int_{\theta^{*}}^{\pi} q \left[ R(\theta) \cos \theta + R'(\theta) \sin \theta \right] d\theta \qquad C_{x} = 2 \int_{0}^{\tau^{*}} q \left[ S(\tau) + S'(\tau) \tau \right] d\tau$$

$$C_{y} \stackrel{\text{or}}{\equiv} 0. \tag{3.2}$$

where the dimensionless pressure is given by

$$q = 1 - \frac{R^2 + R'^2}{R^4} \left[ \frac{\partial \bar{\psi}}{\partial \eta} \bigg|_{\eta=1} + R(\theta) \sin \theta \right]^2 \quad \text{or} \quad q = 1 - \frac{1 + S'^2}{S^2 + \tau^2} \left[ \frac{\partial \bar{\psi}}{\partial \eta} \bigg|_{\eta=0} + \tau \right]^2. (3.3)$$

### 4. Difference Scheme and Algorithm

#### 4.1. Splitting scheme for Laplace equation

For the purposes of the numerical solution, the transformed domain must be reduced to finite one after appropriately choosing the "actual infinities". In the case of polar coordinates the domain is infinite with respect to coordinate  $\eta$  only and it fully enough to select sufficiently large number  $\eta_{\infty}$  and to consider the rectangle:  $[0 \le \theta \le \pi; 1 \le \eta \le \eta_{\infty}]$  (Fig.2a). In the case of parabolic coordinates an actual infinity is to be specified also for the  $\tau$ -coordinate, namely  $\tau_{\infty}$  and to consider the rectangle:  $[0 \le \tau \le \tau_{\infty}; 0 \le \eta \le \eta_{\infty}]$  (Fig.2b). In both directions we employ non-uniform mesh. The first and the last  $\eta$ -lines are displaced (staggered) from the respective domain boundaries on a half of the adjacent value of the spacing. Thus on two-point stencils second-order approximation for the boundary conditions is achieved (see [6]. The non-uniformity of the mesh enables us to improve the accuracy near the body and to reduce the number of points at infinity.

In  $\theta$ -direction the mesh is not staggered but it is once again non-uniform being very dense in the vicinity of the rear stagnation point, i.e. in the vicinity of  $\theta = 0$  which is of crucial importance when acknowledging the infinity in cylindrical coordinates. It is desirable to have the "actual infinity" in cylindrical coordinates as larger as possible in order to prepare the ground for switching to the parabolic coordinates. The connection between the  $\tau$ -mesh and  $\theta$ -mesh is derived on the basis of the connections between the two coordinate systems, namely

$$\tau_j = \sqrt{R(\theta_j)\cos\theta_j + R(\theta_j)}, \quad \text{if} \quad 0 \le \theta_j \le \pi; \qquad S_j = \sqrt{2R(\theta_j) - \tau_j^2},$$
(4.1)

and these relations can be transformed when necessary to calculate  $S_j$ ,  $\tau_j$  from  $R_j$ ,  $\theta_j$  or vice versa.

Due to the topological differences between the polar and parabolic coordinate systems after the transition to parabolic coordinates it is necessary to generate a new  $\tau$ -mesh. The new mesh has to be sparse at large distances behind the body where the gradients of the flow are small. To this end the knots  $\tau_j$  are obtained from (4.1) making use of spline interpolation. The new  $\tau$ -mesh is uniform on the rigid body and is changing behind the body according to the quadratic rule

$$\begin{cases} \tau_j = (j-1)h, & h = \frac{3\sqrt{2}}{N}, \ j = 1, \dots, \left[\frac{N}{3}\right] + 1, \\ \tau_j = \exp\left(j - \left[\frac{N}{3}\right] - 1\right)h\ln\tau_{\infty}, & h = \frac{3}{2N}, \ j = \left[\frac{N}{3}\right] + 2, \dots, N + 1 \end{cases}$$
(4.2)

where  $\left[\frac{N}{3}\right]$  is the last point of the rigid body

We solve the boundary value problem iteratively by means of the method of splitting of operator. Upon introducing fictitious time we render the equation to parabolic type and then employ the so-called scheme of stabilising correction [21]. On the first half-time step we have the following differential equations ( $\Delta t$  is the time increment)

$$\frac{\psi_{ij}^{n+\frac{1}{2}} - \psi_{ij}^{n}}{\frac{1}{2}\Delta t} = \Lambda_2 (b\Lambda_2 \psi^{n+\frac{1}{2}})_{ij} + \Lambda_1 (a\Lambda_1 \psi^n)_{ij} - \Lambda_1 (c\Lambda_2 \psi^n)_{ij} - \Lambda_2 (c\Lambda_1 \psi^n)_{ij}$$
(4.3)

for  $i = 2, \dots, M, j = 2, \dots, N$  with respective boundary conditions [6] The second half-time step consists in solving the following differential equations

$$\frac{\psi_{ij}^{n+1} - \psi_{ij}^{n+\frac{1}{2}}}{\frac{1}{2}\Delta t} = \Lambda_1 (a\Lambda_1 \psi^{n+1})_{ij} - \Lambda_1 (a\Lambda_1 \psi^n)_{ij}$$
(4.4)

for i = 2, ..., M, j = 2, ..., N with respective boundary conditions [6].

Thus the b.v.p. for the stream function is reduced to consequative systems with sparse (tridiagonal) matrices (for detail see e.g.,[6]. The main advantage of the economical schemes of the splitting type is that on each half-time step we solve one-dimensional problems with sparse (tridiagonal) matrices. This can be done by means of the Thomas algorithm [15]. However, the system for streamfunction  $\psi(\eta, \xi)$  cannot be solved by plane Thomas algorithm since the condition for numerical stability of the elimination is not satisfied for all points of domain. For this reason a modification of the Thomas algorithm (in fact Gaussian elimination with pivoting for three-diagonal systems) called "non-monotonous progonka" (see [16], [4]) is employed for its solution.

To calculate afterwards the forces acting upon the body we use the simple formulas for numerical integration based on the trapezoidal rule, which are consistent with the overall second-order approximation of the scheme.

#### 4.2. Difference Approximation for the Free Boundary

The equations (2.7) can be resolved for the derivatives  $R'(\theta)$  or  $S'(\tau)$  when the radicals

exist, i.e. following conditions are satisfied:

$$Q(\theta) \stackrel{\text{def}}{=} \frac{R^2(\theta)}{T^2(\theta)} > 1 , \ T(\theta) = \frac{\partial \bar{\psi}}{\partial \eta} \Big|_{\eta=1} + R(\theta) \sin \theta$$
or
$$Q(\tau) \stackrel{\text{def}}{=} \frac{S^2(\tau) + \tau^2}{T^2(\tau)} > 1 , \ T(\tau) = \frac{\partial \bar{\psi}}{\partial \eta} \Big|_{\eta=0} + \tau ,$$

$$(4.5)$$

where connection between functions T is determined simply by the formula

$$T(\theta) = \frac{1}{2}(S(\tau) - S'\tau)T(\tau) \tag{4.6}$$

The above inequalities are trivially satisfied in the vicinity of the leading-end stagnation point inasmuch as that for  $\theta \to \pi$  (or  $\tau \to 0$ ) one has  $T \to 0$  and hence  $\frac{R^2}{T^2} \to \infty$  or  $\frac{S^2 + \tau^2}{T^2} \to \infty$ . In the present work we use the dynamic condition (2.4) in polar coordinates only, so that we present here just the relevant scheme in polar coordinates without going into the details for parabolic coordinates.

Suppose that the set functions  $\psi_{ij}^{\alpha}$ ,  $R_j^{\alpha}$ ,  $S_j^{\alpha}$ ,  $T_j^{\alpha}$  are known from the previous global iteration, say of number  $\alpha$ .<sup>1</sup> We check the satisfaction of (4.5) beginning from the point  $\theta = 0$  and continue with increasing  $\theta$ . Let  $j^* + 1$  be the last point where (4.5) is satisfied and, respectively  $j^*$  – the first one where it is not (polar coordinates). The position  $\theta^*$  of the detachment point is captured by means of a linear interpolation

$$\theta^* = \frac{\theta_{j^*+1}q_{j^*} - \theta_{j^*}q_{j^*+1}}{q_{j^*} - q_{j^*+1}} \quad \to \quad g^* = \theta^* - \theta_{j^*+1} .$$

For the shape function  $\hat{R}_j$  of free line is solved the following difference scheme

$$\hat{R}_{j-1} - \hat{R}_j = g_j \frac{\hat{R}_j + \hat{R}_{j-1}}{2} \sqrt{\frac{1}{2} \left[ \left( \frac{R_j^{\alpha}}{T_j^{\alpha}} \right)^2 + \left( \frac{R_{j-1}^{\alpha}}{T_{j-1}^{\alpha}} \right)^2 \right] - 1}$$
 (4.7)

for  $j = j^*, \ldots, 2$ , whose approximation is  $O(g_j^2)$ . Only in the detachment point the difference scheme is different, specifying in fact the initial ("inlet") condition, namely

$$\hat{R}_{j^*} - R(\theta^*) = g^* \frac{R(\theta^*) + \hat{R}_{j^*}}{2} \sqrt{\frac{1}{2} \left[ \left( \frac{R_{j^*}^{\alpha}}{T_{j^*}^{\alpha}} \right)^2 + \left( \frac{R(\theta^*)}{T(\theta^*)} \right)^2 \right] - 1} , \tag{4.8}$$

where R without a superscript or "hat" stands for the known boundary of rigid body. Thus the mere condition for existence of the square root of the Bernoulli integral defines at each iteration stage  $\alpha$  the new approximation for the position of the detachment point so that it 'slides' during the iterations alongside the rigid body. This manner of determining of the detachment point we called Christov's algorithm (see [18]).

<sup>&</sup>lt;sup>1</sup>We distinguish here between global and local iteration, the latter referring to the time-stepping of the coordinate splitting method.

In the end a relaxation is used for the shape-function of the free boundary at each global iteration according to the formula:

$$R^{\alpha+1} = \omega \hat{R}_j + (1 - \omega) R_j^{\alpha}$$

where  $\omega$  is called relaxation parameter.

# 4.3. The general Consequence of the Algorithm

Each global iteration contains two stages. On the first stage, the difference problem for Laplace equation is solved iteratively either in polar or in parabolic coordinates (depending on the development of the stagnation zone). The internal iterations (time steps with respect to the fictitious time in the splitting procedure) are conducted until convergence is achieved in the sense that the uniform norm is lesser than  $\varepsilon_2 = 10^{-6}$ . Thus the new iteration for stream function  $\psi_{ij}^{\alpha+1}$  is obtained.

The polar coordinates appear to be instrumental only on the first several (7-10) global iterations. When the rearmost cusp point of the stagnation zone reaches 30–50 diameters of cylinder (calibers), the current-iteration values of the sought functions are transformed to parabolic coordinates and hence the calculations for the stream function continue solely in terms of parabolic coordinates.

The second stage of a global iteration consists in solving the difference problem for the free surface in polar coordinates. The transition to and from parabolic coordinates is done according to (4.1) and (4.6). Note that there is one-to-one correspondence between the points in polar and parabolic coordinates and hence between the respective values of the scalar set functions  $\psi$  and R.

The criterion for convergence of the global iterations is defined by the convergence of the shape function as being the most sensitive part of the algorithm, namely the global iterations are terminated when

$$\max_{j} \left| \frac{R_{j}^{\alpha+1} - R_{j}^{\alpha}}{R_{j}^{\alpha+1}} \right| < 10^{-4}. \tag{4.9}$$

The obtained solutions for the stream function and the shape function of the boundary are the values of the last iteration  $\psi_{ij} = \psi_{ij}^{\alpha+1}$  and  $R_j = R_j^{\alpha+1}$ , respectively. Then the velocity, pressure, and the forces exerted from the flow upon the body are calculated.

### 5. Results and Discussion

The numerical correctness of scheme (4.3), (4.4) is verified through exhaustive numerical experiments and through comparison with the known exact solution for the inviscid non-separated flow past a circular cylinder

$$\psi = U_{\infty}(r - \frac{1}{r})\sin\theta , \qquad (5.1)$$

where  $\psi$  is the stream function,  $U_{\infty}$  – the velocity of the main flow and r and  $\theta$  - the polar coordinates of a point of the flow. We used different meshes with sizes  $M \times N$ :  $41 \times 68$ ,  $41 \times 136$ ,  $161 \times 158$ ,  $101 \times 201$ ,  $101 \times 136$ , etc. Respectively, the actual infinity  $\eta_{\infty}$  assumed in the numerical experiments the values 5, 10, 20. The dependence of the

numerical solution on the time increment  $\Delta t$  is also investigated and it is shown that the approximation of the stationary part of the equations (4.3) and (4.4) does not depend on  $\Delta t$ , i.e. the scheme has the property called by Yanenko [21] full approximation. The relative differences for  $\psi$  when  $\Delta t$  is in the interval [0.001,2] do not exceed 0.5%. The numerical experiments show that the optimal values for  $\Delta t$  is in interval [0.5,1]. For this reason the rest of the calculations in the present work are performed with  $\Delta t = 0.5$ . The comparison of the solution (5.1) to the present numerical results is quantitatively very good. The deviations for the different meshes are in order of approximation  $O(h^2 + g^2)$  and do not exceed 3%. For example in case of mesh  $161 \times 156$  the relative error is about 0.9%.

The adequate choice of the "actual infinities"  $\eta_{\infty}, \tau_{\infty}$  and the spacings  $h_i, g_j$  have a profound impact on the accuracy of the difference schemes (4.3) and (4.4). For a given "actual infinity" the improvement in the accuracy can be achieved through increasing the number of mesh points (decreasing the size of spacing). This makes the use of uniform mesh ineffective because in the far-field region the gradients of the flow are small and the high resolution is not necessary. That was the reason to employ the non-uniform meshes. The "optimal" value for the relaxation parameter turned out to be  $\omega = 0.01$ . Smaller values increased intolerable the computational time while  $\omega > 0.1$  could not ensure the convergence of the global iterations. Respectively  $\eta_{\infty} = 10$  is the optimal value for the lateral "actual infinity"

In order to compare calculated results with the prescription of the Levi-Civita method in case of so called 'critical' separation angle  $\theta_* = 124.2^\circ$  (in respect to leading stagnation point of the cylinder) it is necessary to summarize that method and deduce corresponding relations. Following [1] the physical plane z is mapped on the unit halfcircle t so, that free boundary transforms into the diameter and rigid boundary - into the halfcircumference  $t = e^{i\sigma}, 0 \le \sigma \le \pi$ . Then

$$z = \frac{M}{4} \int_{i}^{t} e^{i\Omega(t)} (1 - it)^{2} \left(1 - \frac{1}{t^{2}}\right) \frac{dt}{t}, \qquad (5.2)$$

where the function  $\Omega(t) = \Theta(t) + i T(t) = \sum_{k=0}^{\infty} a_{2k+1} t^{2k+1}$ . Hence we obtained the following parametrical equations describing boundary of the cylinder from the leading stagnation point to the separation point  $\theta_*$ :

$$x_{cyl}(s) = \mathbf{Re}z = -M \int_{\frac{\pi}{2}}^{s} e^{-\mathrm{T}(t)} \sin \Theta(t) \sin \sigma(1 + \sin \sigma) d\sigma$$

$$y_{cyl}(s) = \mathbf{Im}z = M \int_{\frac{\pi}{2}}^{s} e^{-\mathrm{T}(t)} \cos \Theta(t) \sin \sigma(1 + \sin \sigma) d\sigma ,$$
(5.3)

where  $\frac{\pi}{2} \leq s \leq \pi$ ,  $\Theta(t) = \sum_{k=0}^{12} a_{2k+1} \cos(2k+1)\sigma$ ,  $T(t) = \sum_{k=0}^{12} a_{2k+1} \sin(2k+1)\sigma$ , and parametrical equations describing the freestreamline from the separation point  $\theta_*$  to infinity:

$$x(s) = \mathbf{Re}z = \frac{M}{4} \int_{-1}^{s} \left[ \left( \frac{2}{t} - t - \frac{1}{t^{3}} \right) \cos \Theta(t) - \left( \frac{2}{t^{2}} - 2 \right) \sin \Theta(t) \right] dt + x_{cyl}(\pi)$$

$$y(s) = \mathbf{Im}z = \frac{M}{4} \int_{-1}^{s} \left[ \left( \frac{2}{t} - t - \frac{1}{t^{3}} \right) \sin \Theta(t) + \left( \frac{2}{t^{2}} - 2 \right) \cos \Theta(t) \right] dt + y_{cyl}(\pi),$$
(5.4)

where  $-1 \le s \le 0$ ,  $\Theta(t) = \sum_{k=0}^{12} a_{2k+1} t^{2k+1}$ . If the parameters have values M = 5.71464,  $a_1 = 2$ ,  $a_3 = .12518$ ,  $a_5 = .02661$ ,  $a_7 = .00858$ ,  $a_9 = .00349$ ,  $a_{11} = .00167$ ,  $a_{13} = .00089$ ,  $a_{15} = .00053$ ,  $a_{17} = .00035$ ,  $a_{19} = .00024$ ,  $a_{21} = .00018$ ,  $a_{23} = .00016$ , it corresponds to the so called critical separated flow, which detaches at angle  $\theta_*$ . This Helmholtz flow has decreasing (concave) stagnation zone with cusp end at infinity (Chaplygin–Kolscher flow).

Further the velocity

$$v(z) = \frac{1+it}{1-it}e^{-i\Omega(t)}$$
, from where  $|v(z)| = \frac{\cos\sigma}{1+\sin\sigma}e^{T(t)}$ , (5.5)

whence it follows immediately that the pressure on the cylinder is

$$p(\theta) = 1 - |v|^2 \,, \tag{5.6}$$

where  $\theta = \arctan \frac{y_{cyl}(s)}{1 - x_{cyl}(s)}$  is the polar angle.

In Figs.3-a,b are presented the obtained shapes of the stagnation zone behind the cylinder and in the near wake for resolutions  $41 \times 68$ ,  $81 \times 136$  and  $101 \times 201$  and different values of relaxation parameter:  $\omega = 0.01; 0.001$ . Obviously there is an excellent comparison between different numerical realizations. On the same figure is added the shape of the Chaplygin-Kolscher flow. The latter we calculate by means of parametrical equations (5.3), (5.4) using the usual trapezoidal rule. The symbols stand for the results taken from the charts of the paper [17]. It is worth noting the perfect coincidence of the computed by us separation angle with both this one, computed in [17] and the 'critical' one, prescribed by the hodograph (Levi-Civita's) method. Nevertheless the difference between our solution and this in [17] is sizable due to the inconclusive character of the latter. The logarithmic scale is used in Fig.3-b in order to expand the differences between the different difference solutions making them visible in the graph. The shapes of the free boundary obtained on the three grids with different resolution are compared among themselves very well up to 200 calibers. It is clearly seen up to 70 calibers the shapes are practically indistinguishable and up to 160–170 calibers the relative difference does not exceed 1-3% respectively. This supports the claim that indeed a solution to the Helmholtz problem has been found numerically by means of the developed in the present work difference scheme. At the Fig.3-b it is seen the quantitative difference between our numerical solution of cusp-ended type and this one prescribed by the hodograph method. Indeed there is excellent agreement concerning the positions of detachment point and pressure distribution but the hodograph method postulates the asymptotic behaviour of the free line also. On the contrary we do not set any condition at infinity. In a sense our free boundary has an implicit numerical "closure" of cusp-ended type.

The calculated dimensionless pressure q is shown in Fig.4. Here is seen again an excellent comparison among the different mesh resolutions. In the stagnation zone it is in order of  $10^{-4}$ , which is in very good agreement with the assumption that the unknown boundary is defined by the condition q = 0. The amplitude of the minimum of q is smaller than 3 the latter being the value for ideal flow without separation. This means that the stagnation zone influences on the flow upstream. On the same figure is presented the pressure, calculated by means of (5.6) which corresponds to the separation angle  $\theta_* = 124.2^o$ . Apparently obtained here pressure approximates very well this curve. It

is known the Chaplygin-Kolscher flow has a vanishing drag coefficient [1, 10]). In other words there exists an inviscid separated flow submitted to The D'Alembert paradox like nonseparated. Varying the mesh parameters we obtained for the drag coefficient  $C_x$  values between  $2 \times 10^{-2}$  when resolution is  $41 \times 68$  and  $5 \times 10^{-4}$  when resolution is  $101 \times 201$ . That is to say our  $C_x \approx 0$  and the error is in order of approximation. In order to confirm the above assumption we made the following numerical experiment: in formula (3.2) for the drag coefficient we replaced our pressure by the pressure obtained from (5.6). The calculated value is  $C_x = 3 \times 10^{-4}$ .

# 6. Concluding Remarks

An algorithm for numerical solving the classical Helmholtz problem behind a circular cylinder is developed. Scaled coordinates are employed rendering the computational domain into a region with fixed boundaries and transforming the Bernoulli integral into an explicit equation for the shape function. The crucial feature of the method developed here is that the detachment point is not prescribed in advance. Rather it is defined iteratively. Difference scheme using coordinate splitting is devised. Exhaustive set of numerical experiments is run and the optimal values of scheme parameters are defined. Results are verified on grids with different resolutions. The drag coefficient of the calculated separated flow vanishes like cusp-ended infinite flow obtained by means of the hodograph method.

**Acknowledgments** The author presents his gratitudes to Prof. C.I. Christov for the many helpful discussions and support allowing this work to be carried out.

The financial support by the National Science Foundation of Bulgaria, under Grant MM-602/96 is gratefully acknowledged.

#### References

- [1] G. Birkhoff and E. H. Zarantonello. *Jets, Wakes, and Cavities*. Academic Press, New York, 1957.
- [2] S. Brodetsky. Discontinuous fluid motion past circular and elliptic cylinders. *Proc. Roy. Soc.*, *London*, A718:542–553, 1923.
- [3] S. A. Chaplygin. On the jets in an incompressible fluid. *Proc.Division Phys.Sci.*, *Society of the Natural Sci. Adherens*, X, edit.1, 1899. See also Collected works, Gostehizdat, Moskow-Leningrad, 1:5–18, 1948 (in Russian).
- [4] C. I. Christov. Gaussian elimination with pivoting for multi-diagonal systems. Internal Report 4, University of Reding, 1994.
- [5] C. I. Christov and M. D. Todorov. Numerical investigation of separated or cavitating inviscid flows. In *Proc. Int. Conf. Num. Methods and Applications, Sofia 1984*, pages 216–233, 1985.
- [6] C. I. Christov and M. D. Todorov. On the determination of the shape of stagnation zone in separated inviscid flows around blunt bodies. In *Proc. XV Jubilee Session on Ship Hydrodynamics, Varna*, 1986, page paper 10, Varna, 1986. BSHC.
- [7] C. I. Christov and M. D. Todorov. An inviscid model of flow separation around blunt bodies. *Compt. Rend. Acad. Bulg. Sci.*, 7:43–46, 1987.
- [8] C. I. Christov and M. D. Todorov. Numerical approach to imviscid separated flows with infinitely long cusp ended stagnation zone. In *Proc.XXII Summer School "Application of Mathematics in Engineering"*, Sozopol, 14-21.9.1996, pages 88-97, Sofia, 1997.

- [9] C. I. Christov and P. Volkov. Numerical investigation of the steady viscous flow past a resting deformable buble. *J. Fluid Mech.*, 153:341–364, 1985.
- [10] M. I. Gurevich. The theory of jets in an ideal fluid. Nauka, Moscow, 1979. in Russian.
- [11] H. Helmholtz. Uber discontinuirliche flussigkeitsbewegnungen. Monatsbericht. d. Akad. d. Wiss., (Berlin):215–228, 1868.
- [12] I. Imai. Discontinuous potential flow as the limiting form of the viscous flow for vanishing viscosity. J. Phys. Soc. Japan, 8(No 3):399–402, 1953.
- [13] G. Kirchhoff. Zur Theorie freier Flussigkeitsstrahlen. J. Reine Angew. Math., 70:289–298, 1869.
- [14] T. Levi-Civita. *Scie e leggi di resistenza*, volume t.II 1901-1907, pages 519–563. Publ. a cura dell Acad. naz. dei Lincei, Bologna, 1956.
- [15] P. J. Roache. Computational Fluid Dynamics. Hermosa, 1972.
- [16] A. A. Samarskii and E. N. Nikolaev. Numerical Methods for Grid Equations. Nauka, Moskow, 1978. in Russian. English translation: Birkhauser, Basel, 1989.
- [17] R. V. Southwell and G. Vaisey. Fluid motions characterized by 'free' stream-lines. *Phil. Trans.*, A240:117–161, 1946.
- [18] M. D. Todorov. Christov's algorithm for Helmholtz problem: an integral—equations implementation. In Proc.XVIII National Summer School "Application of Mathematics in Technology", Varna, 25.8.-2.9.1992, pages 191-193, Sofia, 1993.
- [19] H. Villat. Sur la resistance des fluides, Apercus theoriques. Number 38. Gauthier-Villars, Paris, 1920.
- [20] T. Y. Wu. Cavity and wake flows. Ann. Rev. Fluid Mech., 4:243-284, 1972.
- [21] N. N. Yanenko. Method of Fractional Steps. Gordon and Breach, 1971.

#### FIGURE CAPTIONS

fig1.gif

Figure 1: Posing the problem

fig2a.gif

Figure 2a

fiq2b.qif

Figure 2b

cylsnear.gif

(a) behind the cylinder

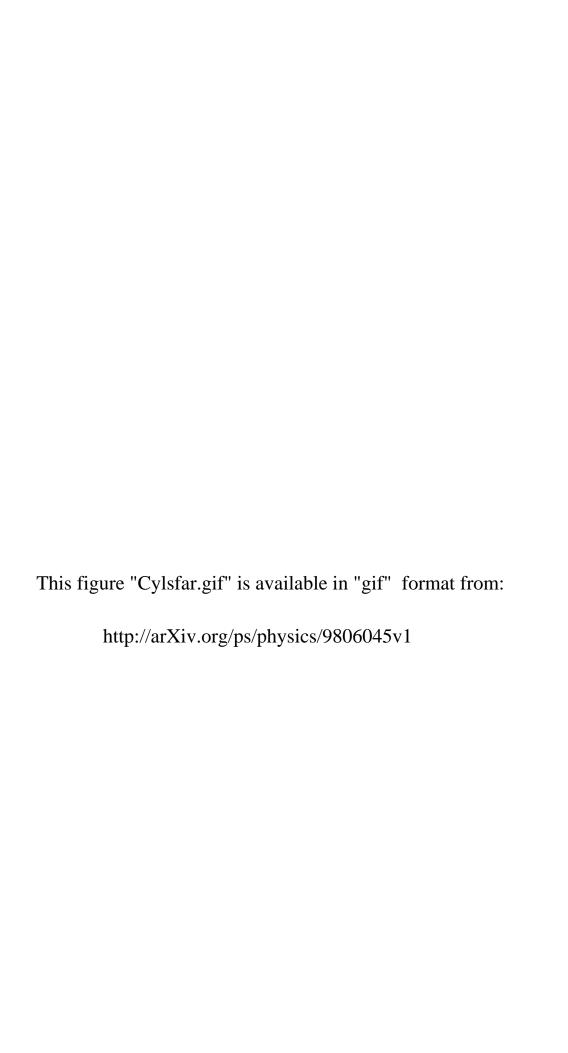
cylsfar.gif

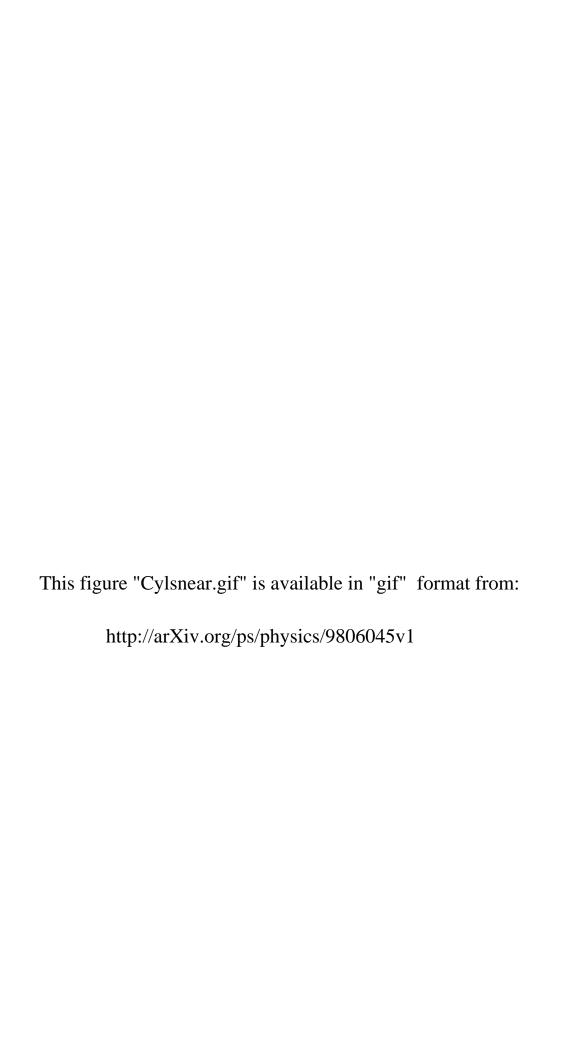
(b) far wake

Figure 3: The obtained separation lines for relaxation parameter  $\omega = 0.01$  and different resolutions: - - - - 41 × 68; — — 81 × 136; - - - 101 × 201; — hodograph method;  $\triangleright \triangleright \triangleright \triangleright$  [17]

prescyls.gif

Figure 4: The pressure distribution for relaxation parameter  $\omega = 0.01$  and different resolutions: - - - -  $41 \times 68$ ; — —  $81 \times 136$ ; — -  $101 \times 201$ ; — hodograph method;  $\circ \circ \circ \circ$  nonseparated inviscid flow.





This figure "Fig1.gif" is available in "gif" format from:

http://arXiv.org/ps/physics/9806045v1

This figure "Fig2a.gif" is available in "gif" format from:

http://arXiv.org/ps/physics/9806045v1

This figure "Fig2b.gif" is available in "gif" format from:

http://arXiv.org/ps/physics/9806045v1

